RSC Advances

ROYAL SOCIETY OF CHEMISTRY

www.rsc.org/advances

Cite this: DOI: 10.1039/c0xx00000x

www.rsc.org/xxxxxx

ARTICLE TYPE

Gentamicin-loaded carbonated hydroxyapatite coatings with hierarchically porous structures: drug delivery property, bactericidal property and biocompatibility

Sha Tang[a,1], Bo Tian[b,1], Qin-Fei Ke[a], Zhen-An Zhu[b]*, Ya-Ping Guo[a]*

Received (in XXX, XXX) Xth XXXXXXXXX 20XX, Accepted Xth XXXXXXXXX 20XX
DOI: 10.1039/b000000x

Carbonated hydroxyapatite coatings (CHACs) on titanium alloy substrates have been widely used as bone substitute materials. However, implant-associated infection becomes a serious problem in orthopedic surgery, leading to prolonged antimicrobial treatment, extensive bone debridement and failure of implants. Herein, gentamicin-loaded CHACs (Gent-CHACs) were fabricated according to the following steps: (i) the conversion of CHACs with hierarchically porous structures from calcium carbonate coatings (CCCs) by treatment with phosphate buffer solutions, and (ii) loading gentamicin into the CHACs. Main constituents in the CHACs were plate-like carbonated hydroxyapatite particles with a low crystallinity. Mesopores with a pore size of ~3.8 nm and macropores (or apertures) with an aperture size of ~1 μm existed within and among the plates, respectively. The hierarchically porous structures made the CHACs possess good drug loading-release properties. The sustained release of gentamicin from the Gent-CHACs inhibited significantly bacterial adhesion and prevented biofilm formation against *S. epidermidis* (ATCC35984). *In vitro* cell tests indicated that human bone marrow stromal cells (hBMSCs) had good cell adhesion, spreading and proliferation on the Gent-CHACs. Moreover, the released gentamicin from the Gent-CHACs had no toxic effects on the hBMSCs. The good biocompatibility, drug delivery property and bactericidal property of the Gent-CHACs suggest that they have great potentials as bone substitute materials.

1. Introduction

Total joint arthroplasty is a highly reliable and cost-effective method to treat severe arthritis in hip and knee. In the United States nearly 700,000 hip and knee arthroplasty is performed annually with demand predicted to increase substantially.[1] Notably, post-surgery implant-associated infection still remains a threat in the field of total joint orthopedic surgery, leading to prolonged antimicrobial treatment, extensive bone debridement and failure of implant. The rate of infection is approximately 4.3% among all orthopedic implant surgeries.[2] Common therapeutic method of implant-associated infection is a systemic antibiotic administration by injection and oral ingestion. However, it is difficult to achieve effective localization of antibiotics, and high concentrations of antibiotics may result in the risk of systemic toxicity. Moreover, this therapy is often ineffective when adherent bacteria form biofilms on the surfaces of prosthesis. Therefore, ideal bone substitution materials should not only possess good biocompatibility, biodegradability and bioactivity, but also have good drug delivery property and bactericidal property without any systemic toxicity.

Carbonated hydroxyapatite coatings (CHACs) on titanium alloy substrates are widely used for bone substituted materials especially under load-bearing conditions, because they combine the mechanical advantages of titanium alloys with the excellent biological property of carbonated hydroxyapatite.[3] Unfortunately, conventional CHACs have limited drug loading capacities (DLCs) because of none porous structure and low surface area. In 2001, silica-based mesoporous materials as drug delivery systems were reported for the first time to confine ibuprofen because of their great specific surface area, large pore volume, and low-toxic nature.[4] The main disadvantages of silica-based mesoporous materials are low bioactivity and biodegradability, so they should be removed by a second surgical operation.[5] An alternative strategy is to fabricate mesoporous hydroxyapatite or mesoporous bioactive glasses.[6] Mesoporous carbonated hydroxyapatite not only shows the compositional similarities to bone minerals,[7] but also its mesoporous structure makes it possible to incorporate high dosages of drugs and release them at a controlled rate.[8] Recently, mesoporous hydroxyapatite particles are fabricated by using non-ionic surfactants and ionic surfactants as soft templates.[9] Such materials possess large surface areas, pore volumes and ordered mesoporous channels, but the remained surfactants may reduce their biological property. In our previous work, we fabricated the CHACs with hierarchically porous structures according to the following steps:

(i) depositing calcium carbonate coatings (CCCs) on Ti6Al4V substrates by electrophoresis; and (ii) converting the CCCs to the CHACs with hierarchically porous structures by treatment with a phosphate buffer solution (PBS).[10] Simulated body fluid immersion tests revealed that the CHACs possessed good *in vitro* bioactivity due to calcium deficiencies in apatite lattice and hierarchically porous structures.[10a]

Gentamicin is widely used as an antibiotic to prevent implant-associated infections because of its low cost, good stability and broad spectrum of antibacterial activity.[11] However, gentamicin for intramuscular (or intravenous) injection and oral ingestion is not effective, because the drug cannot readily reach necrotic or avascular tissues. Moreover, high dosages and frequent systemic administration of gentamicin may induce severe side effects such as nephrotoxicity and ototoxicity.[12] An ideal strategy is to fabricate the biocoatings which possess good drug loading-release property. The release of drugs from the biocoatings can inhibit significantly bacterial adhesion and prevent biofilm formation.

In the present work, we successfully prepared gentamicin-loaded CHACs (Gent-CHACs) according to the following steps: (i) formation of the CHACs with hierarchically porous structures from CCCs by treatment with PBS, and (ii) loading gentamicin into the CHACs by lyophilization method. The main aim was to investigate the drug loading-release property of the CHACs, and to study the bactericidal property of the Gent-CHACs against S. epidermidis (ATCC 35984). Moreover, *in vitro* biocompatibility and cellular response of the Gent-CHACs were investigated by using human bone marrow stromal cells (hBMSCs) as cell models.

2. Experimental

2.1. Preparation of CHACs

The Ti6Al4V substrates (Northwest Institute for Non-ferrous Metal Research) were mechanically ground with 1000-grit silicon carbide paper followed by a chemical corrosion treatment in a 1.0 mol/L H_3PO_4-1.5 $_{wt}$% HF solution (AR, Sinopharm) for nearly 20 min, then the substrates were washed with deionized water and dried in air. 1.25 g of $CaCO_3$ powders (AR, Aladdin) were immersed into 250 ml of ethanol. The mixture was dispersed for 30 min under ultrasonic conditions to get a suspension solution. The Ti6Al4V was used as the cathode and a graphite plate was used as the anode. The two electrodes were kept about 10 mm apart. The electrophoretic process was carried out at 90 V for 1 min by using 0.5 ml of a 1.0 mol/L HCl solution (AR, Sinopharm) as the additive.

In order to prepare PBS with a concentration of 0.2 mol/L, 35.82 g quantity of $Na_2HPO_4 \cdot 12H_2O$ (AR, Sinopharm) and 15.60 g of $NaH_2PO_4 \cdot 2H_2O$ (AR, Sinopharm) were dissolved in 500 ml of deionized water. The CCCs were immersed into the above PBS (pH=7.4) for 3 days at 37 ^oC. To keep the pH value at 7.4, the PBS was replaced every day. Finally, the products (CHACs) were washed with deionized water, and dried in a convection oven at 37^oC for 48 hours.

2.2. Characterization of CHACs

The morphologies of specimens were investigated by scanning electron microscopy (SEM, XL800, Philips). The crystalline phases of the specimens were examined with X-ray powder diffraction (XRD, D8, Bruker) using CuKα radiation within the scanning range of 2θ =20^o to 60^o. Fourier transform infrared spectra (FTIR, 5DX, Nicolet) were carried out to analysis the functional groups at the wavenumber range of 4000-400 cm^{-1} by using the KBr pellet technique. N_2 adsorption-desorption isotherms were measured with an automatic surface area and porosity analyzer (AUTOSORB-1-C, Quantachrome) at -203.85 ^oC. The pore size distributions were derived from desorption branches of isotherms by using the Barrett-Joyner-Halanda (BJH) method.

2.3. *In vitro* drug loading and release study

The Ti6Al4V plates and CHACs were filled with gentamicin by a simplified lyophilization method.[13] In brief, gentamicin (Sigma) was dissolved in a phosphate buffer solution (PBS). The Ti6Al4V plates and CHACs surfaces were cleaned with deionized water. 20 μl of gentamicin solution containing with 150 μg or 300 μg was respectively added onto the material surfaces, and gently spread to ensure even coverage. The surfaces were allowed to dry under vacuum for 2 h. In this way, the Ti6Al4V plates and CHACs were loaded with 150 μg or 300 μg of gentamicin, and were denoted as Gent-Ti(150 μg), Gent-Ti(300 μg), Gent-CHACs(150 μg) and Gent-CHACs(300 μg), respectively. After the final drying step, the surfaces were rinsed quickly by 1 ml of PBS three times to remove the excess drug. The rinse solutions were collected and stored for further analysis.

The Gent-Ti and Gent-CHACs were immersed in 1 ml of PBS with pH=7.4 in a 12-well plate at room temperature. The release medium was withdrawn at predetermined time intervals, and replaced with 1 mL fresh PBS at each measurement to determine the release kinetics. Samples were collected periodically for up to 24h. The drug concentrations of the gentamicin-release medium were analyzed by using an *o*-phthaldialdehyde method.[14] In brief, the *o*-phthaldialdehyde reagent was formulated by adding 2.5 g of *o*-phthaldialdehyde (Sigma), 62.5 ml of methanol (Sigma) and 3ml of 2-mercaptoethanol (Sigma) to 560ml of sodium borate (Sigma) in distilled water solution. The reagent was stored in a brown bottle in a dark chamber for at least 24 h. This reagent could be used for only 3 days, and then it started degrading. The collected gentamicin solution, *o*-phthaldialdehyde reagent and isopropanol were mixed in similar proportions and stored for 30 min at room temperature. The *o*-phthaldialdehyde reacted with gentamicin amino groups to form chromophoric products, whose absorbances were measured at 332 nm. A standard curve with known concentrations of gentamicin was used to determine the unknown concentrations.

2.4. Bacterial culture and bactericidal effect of Gent-CHACs

Bacterial cell line of *S. epidermidis* (ATCC35984) was obtained in freeze-dried form from the American Type Culture Collection (ATCC). The cells were propagated on an agar plate for 3 days before transferring them to BBL^{TM} Trypticase^{TM} Soy Broth (TSB, BD Bioscience, USA, pH=7.4). Before bacterial seeding, bacteria were withdrawn from the plates by using a sterile 10 μl loop and inoculated in a polystyrene tube with 3ml of broth. The tube was agitated for approximately 12-16 h (overnight culture) on a shaker at 150 rpm and 37˚C. Bacteria concentrations were assessed by optical density. For this purpose, the broth–bacteria

solution was diluted in different ratios, and the transmittance was measured by using a spectrophotometer. According to McFarland standards, the concentration of bacteria solution with 30% transmittance is 900 million bacteria/ml. Further dilutions were performed with broth upon to the final concentration of 10 million bacteria/ml.

The antibacterial properties of the Ti6Al4V plates, the Gent-Ti(150 μg), Gent-Ti(300 μg), CHACs, Gent-CHACs (150 μg) and Gent-CHACs (300 μg) were analyzed by using the spread plate method as described in our previous report, respectively.[15] ATCC35984 strains were prepared by adjusting the concentration to 1×10^6 cfu/mL in TSB. 1mL of the suspension was added to a 12-well plate that contained different samples, and was incubated at 37˚C for 24 h. The samples were collected, gently washed with sterile PBS for three times to remove the loosely adherent bacteria, and placed into glass tubes with 0.5 mL of TSB. The adherent bacteria on the samples were dislodged by ultrasonication (20 min) in a 150 Ultrasonic bath (B3500S-MT, Branson Ultrasonics Co., Shanghai, China) at a frequency of 50 Hz. The solutions were serially diluted 10-fold. 0.5 mL of each suspension were plated in triplicate onto BBL tryptone soy agar (TSA) and then incubated at 37˚C for 24 h. The mean surviving numbers of colonies on the TSA were calculated. The group of Gent-Ti was included as a positive control.

Similar to the spread plate method, the Ti6Al4V plates, Gent-Ti(150 μg), Gent-Ti(300 μg), CHACs, Gent-CHACs (150 μg) and Gent-CHACs (300 μg) were gently washed three times with PBS. Subsequently, the samples were stained in a new 12-well plate with 300μl combination dye (LIVE/DEAD Baclight bacteria viability kits, Molecular Probes, L13152) and analyzed with confocal laser scanning microscope (CLSM, Leica TCS SP2; Leica Microsystems, Heidelberg, Germany). The viable and nonviable cells were distinguished under fluorescence microscope. The viable bacteria with intact cell membranes appeared fluorescent green, whereas nonviable bacteria with damaged membranes appeared fluorescent red.

The formation of bacterial biofilms was observed by using scanning electron microscopy (SEM) (JEOL JSM-6310LV, JEOL Ltd., Tokyo, Japan). After 24h of incubation, the samples were prepared for SEM observation according to the following standard procedures. The samples were gently washed three times with PBS to remove non-adherent bacteria. The biofilms were fixed in 2.5% glutaraldehyde for 2 h at 4 ºC, washed three times with cacodylate buffer, and dehydrated through a series of graded ethanol solutions (50%, 60%, 70%, 80%, 90%, 95% and 100%). The samples were subsequently freeze-dried, sputter coated with gold, and observed by using SEM.

Bacterial biofilms were stained with crystal violet using a modification of the method of O'Toole et al.[16] Specifically, ATCC35984 strains were prepared by adjusting the concentration to 1×10^4 cfu/mL in TSB. 0.5 mL of the suspension were statically incubated in 12-well plates containing the Ti6Al4V plates, Gent-Ti(150 μg), Gent-Ti(300 μg), CHACs, Gent-CHACs (150 μg) and Gent-CHACs (300 μg) for 2, 5, and 8 h at 37 ºC. The medium containing non-adherent bacteria was carefully removed, and the samples were moved to fresh wells. These samples were washed for 6 times with PBS and then stained, in a new well, with 1 mL of PBS containing 100 mL of 1 wt/v% crystal violet (Sigma- Aldrich, St. Louis, MO) and incubated for 15 minutes at room temperature. The samples in the wells were washed for 3 times with PBS and crystal violet, and then were dissolved by addition of 2 mL of 95% EtOH, with rocking for 15 minutes. Absorbance was measured at 570 nm by using an automated plate reader (Perkin-Elmer).

2.5. Cell behaviour of Gent-CHACs

The study was approved by the Ethic Committee of the Ninth People's Hospital of Shanghai Jiao Tong University. The hBMSCs were isolated and expanded by using a modification of standard methods as described previously.[17] The donor was healthy without metabolic disease, inherited illnesses or other diseases that might affect the current study. Cells were grown in complete Alpha Minimum Essential Medium (α-MEM; GIBCO, Grand Island, NY, USA) supplemented with 10% fetal bovine serum (FBS; Hyclone, Tauranga, New Zealand) and antibiotics (penicillin 100 U/mL, streptomycin 100 mg/mL; GibicoBRL, Grand Island, NY). The hBMSCs were incubated at 37°C in a humidified atmosphere of 5% CO_2 and 95% air, with the growth medium changed every 48h. The hBMSCs from passage 3 to 5 were detached by 0.25% trypsin, resuspended in a different density using fresh culture medium, and used for the experiments described below.

The cell morphology and spreading of hBMSCs on the Ti6Al4V plates and Gent-CHACs(300 μg) were investigated by detecting cytoskeletal filamentous actin. Briefly, hBMSCs were seeded on the Ti6Al4V plates and Gent-CHACs(300 μg) at a density of 3×10^4 cells/sample in a 12-well plate in triplicate, respectively. After 24 h of incubation, the samples were gently washed with PBS and maintained in 4 % paraformaldehyde for 15 min, followed by immersing in 0.1 % Triton X-100 solution for 15 min. tetramethylrhodamine-6-isothiocyanate (TRITC) phalloidin was used to stain actin filaments of hBMSCs as red fluorescent light, and 4',6-diamidino-2-phenylindole (DAPI) was used to stain nuclei shown as blue fluorescent light. Cell morphology and spreading were visualized by using CLSM

The hBMSCs were seeded on the Ti6Al4V plates and Gent-CHACs(300 μg) at a density of 7×10^3 cells/sample in a 12-well plate after culturing for 12 h, 1 day, 3 days, 5 days and 7 days, respectively. The number of viable cells was measured with cell counting kit-8 (CCK-8, Dojindo, Kumamoto, Japan). At each time point, 100 μL of water-soluble tetrazolium-8 solution was added to each well, and samples were incubated for 2 h at 37°C. 200 μL of solution for each well was added into a new 96-well plate and absorbance was measured at 450 nm by a microplate spectrophotometer (Bio-Rad Laboratories, Hercules, CA).

2.6. Statistical analysis

Data are presented as the mean ± standard deviation (S.D.) from at least three independent experiments. Statistical analysis was performed by Student's t-test using the SPSS 13.0 software (SPSS Inc., USA). Difference were considered significant at $*P < 0.05$ or $**P < 0.01$.

3. Results and discussion

3.1. Phase, morphology and mesoporous structure of CHACs

Titanium alloys have great potentials for orthopedic surgery

because of their excellent mechanical property and biocompatibility.[18] Unfortunately, titanium alloys are bio-inert materials which can not directly bond to bone immediately, and do not possess bactericidal property to treat implant-associated infection. To overcome the above drawbacks, we developed CHACs with hierarchically porous structures, which could be used as bone substitute materials and serve as local drug delivery systems to achieve anti-infection property.

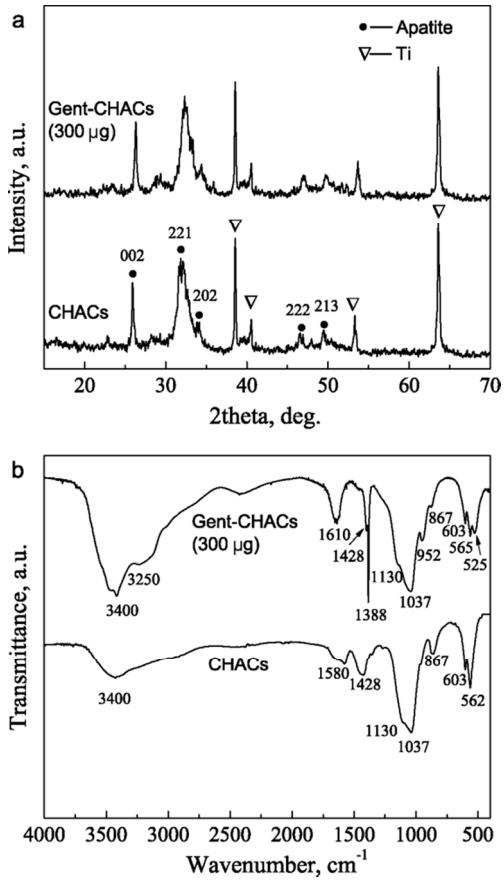

Fig. 1 (a) XRD patterns and (b) FTIR spectra of CHACs and Gent-CHACs (300 μg).

The CHACs were fabricated according to the following steps: (i) formation of the CCCs on Ti6Al4V substrates by electrophoresis; and (ii) conversion of the CHACs from the CCCs by treatment with PBS.[10a] The phases of the calcium carbonate particles on the CCCs were calcite and vaterite. After soaking in PBS for 3 days at 37°C, the CCCs were converted into the CHACs via a dissolution-precipitation reaction.[10a] In order to make the CHACs possess achieve anti-infection property, gentamicin was loaded on the CHACs to form Gent-CHACs by the simplified lyophilization method.[13] The XRD pattern in Fig. 1a indicated that the main phase of both the CHACs and Gent-CHACs(300 μg) was hydroxyapatite. The intensity ratio between (002) and (211) diffraction was stronger than the standard diffraction pattern (JCPDS card no. 09-0432), demonstrating that the preferential growth of the hydroxyapatite along the *c*-axis during the reaction process of calcium carbonate to hydroxyapatite. The broad characteristic peaks indicated that the hydroxyapatite had low crystallinity, which could be possibly attributed to the presence of an amorphous mineral phase.[19] However, no characteristic peaks corresponding to gentamicin were detected because of its low percentage of gentamicin in the Gent-CHACs. In addition, Fig. 1a shows the characteristic peaks of Ti derived from Ti6Al4V substrates.

Fig. 1b shows the FTIR spectra of the CHACs and Gent-CHACs. The characteristic absorption peaks of hydroxyapatite were detected in the two samples. The intense absorption peak at 1037 cm^{-1} was ascribed to the stretching vibration (v_3) of the phosphate (PO_4^{3-}) groups, and the peaks at 562, 603 cm^{-1} were ascribed to the bending vibration (v_4) of the phosphate (PO_4^{3-}) groups.[20] The characteristic absorption band due to HPO_4^{2-} at around 1130 cm^{-1} indicated that the apatite in the CHACs and Gent-CHACs was calcium-deficient hydroxyapatite. The band of stretching vibration of OH group or absorbed water was observed at 3400 cm^{-1}.[20] Additionally, the characteristic bands of B-type CO_3^{2-} substitution were detected at 867 cm^{-1} (v_2) and 1428 cm^{-1} (v_3), suggesting that the PO_4^{3-} ions in the apatite crystals were replaced partly by the CO_3^{2-} ions.[21] These results suggested that the general formula of apatite in the CHACs and Gent-CHACs might be express as $Ca_{10-x-y/2}(HPO_4)_x(PO_4)_{6-x-y}(CO_3)_y(OH)_{2-x}$. As compared with the CHACs, the characteristic peaks due to gentamicin were detected in Gent-CHACs (300 μg) (Fig. 2b). The band at 3250 cm^{-1} was attributed to $-NH_2$ bond stretching, and the band at 1610 cm^{-1} was attributed to the N-H group bending. C-N stretching vibration at around 1030 cm^{-1} was overlapped by the stretching vibration of phosphate groups in hydroxyapatite. Owing to the presence of gentamicin in the Gent-CHACs, the peak at 562 cm^{-1} due to PO_4^{3-} groups was split into two peaks at 565 and 525 cm^{-1}. These above results demonstrated that gentamicin was successfully loaded on the CHACs.

Our previous work revealed that calcium carbonate particles with a particle size of 0.5-10 μm deposited on the Ti6Al4V substrates by electrophoretic deposition. These particles in the CCCs were stacked loosely together due to the weak electrostatic bonding, and thus they easily fell off from the coatings.[10a] Interestingly, the calcium carbonate particles in the CCCs were converted *in situ* to carbonated hydroxyapatite via a dissolution-precipitation reaction after treatment of PBS for 3 days (Fig. 1). The SEM images of the CHACs in Fig. 2a indicated that plate-like carbonated hydroxyapatite particles were formed with vertical growth from the particles. The aggregates of these carbonated hydroxyapatite plates resulted in the formation of connected macropores with a size of about 0.2~1 μm (Fig. 2b). These macropores may highly improve the specific surface area of the coatings, and are beneficial for the drug diffusion to the inner site of the coatings, leading to improving their high drug delivery capacity. The corresponding EDS spectrum of the coatings is shown in Fig. 2c. The chemical elements of the CHACs were mainly composed of Ca, P, O, C, and Na elements. The Ca, P and O elements were derived mainly from the hydroxyapatite in the CHACs. The C element was attributed to the CO_3^{2-} which was inclined to substitute PO_3^{4-} in the apatite lattice. The Na element was attributed to either the adsorbed Na^+ from PBS or the part substitution of Ca^{2+} by Na^+ in the crystal lattice. The average Ca/P molar ratio of the carbonated hydroxyapatite was about 1.56, which was lower than that of stoichiometric hydroxyapatite (Ca/P=1.67). The above result

suggested that the carbonated hydroxyapatite was calcium-deficient apatite, as confirmed by the FTIR spectrum (Fig. 1b). The TEM image revealed that the plates in the CHACs were composed of many smaller nanocrystals with a particle size of 4-6 nm, as confirmed by the light-shaded spots (Fig. 2d). The aggregates of these nanocrystals resulted in forming mesopores among them. The electron diffraction pattern in Fig. 2e showed clearly visible diffraction rings, which were in good agreement with the characteristic spacings of an apatite-like structure. The mesoporous structure of the CHACs was confirmed by the N_2 adsorption-desorption isotherm and the corresponding BJH pore size distribution curve (Fig. 2d). According to International Union of Pure and Applied Chemistry (IUPAC), the CHACs had a type IV isotherm with a H3-type hysteresis loop deriving from nanoparticle aggregates with slit-shaped pores (Fig. 2d). The corresponding BJH pore size distribution curve indicated that the pore size was mainly distributed around 3.8 nm (Fig. 2d, inset). The steep increase of nitrogen adsorption at P/P_o 0.9-1.0 suggested the presence of macropores, which was consistent with the SEM images (Fig. 2b). The BET surface area and pore volume of the CHACs were 43.03 m^2/g and 0.112 cm^3/g, respectively. The CHACs possessed a large surface area and high pore volume, so they had great potentials for drug delivery applications.

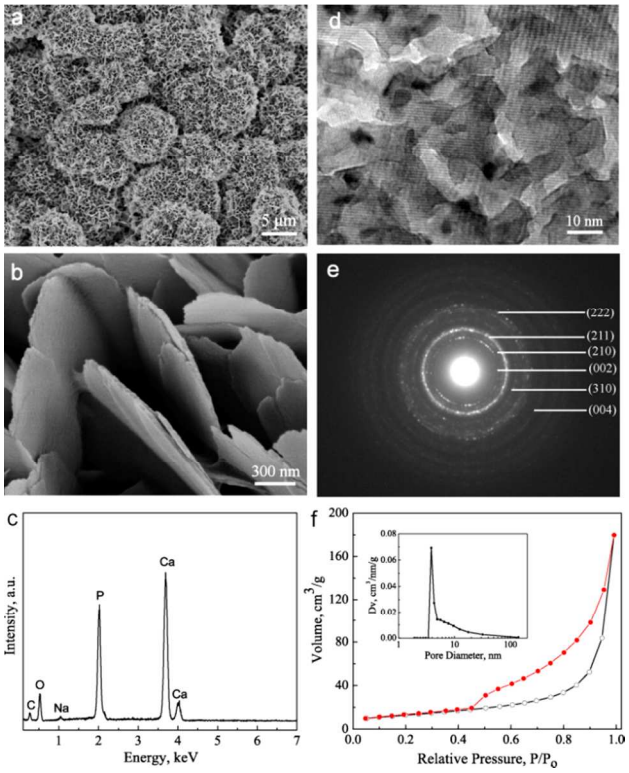

Fig. 2. (a,b) SEM image, (c) EDS spectrum, (d) TEM image, (e) ED pattern and (d) N_2 adsorption-desorption isotherm of CHACs. The inset in (f) showed the BJH pore size distribution.

The SEM images of Gent-CHACs (300 μg) are shown in Fig. 3. The morphologies of the Gent-CHACs (300 μg) was much similar to those of the CHACs (Figs. 2a and 3a). Although the FTIR spectra demonstrated that gentamicin was loaded on the CHACs (Fig. 1b), no gentamicin materials were detected in the SEM images (Fig. 3b). The reason was attributed to the uniform dispersion of gentamicin on the hydroxyapatite plates rather than the aggregation of gentamicin on the coatings.

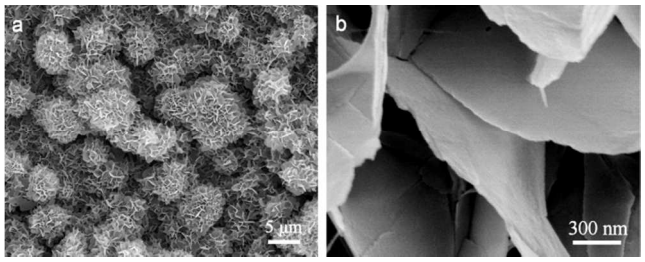

Fig. 3. SEM images of Gent-CHACs (300 μg): (a) low- magnification image and (b) high- magnification image.

3.2 Drug delivery property of CHACs

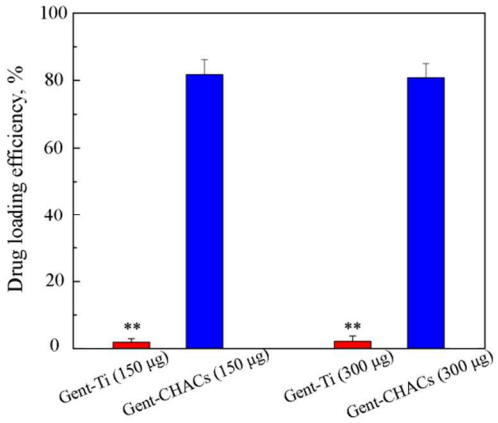

Fig. 4 Drug loading efficiencies of Ti6Al4V plates and CHACs loaded with different drug concentrations. The data were represent as mean ± standard deviation; n=3. $^{**}P < 0.01$.

Implant-associated infection becomes a serious problem in orthopedic surgery. One of the most effective treatment methods is to introduce a controlled antibiotic delivery system, achieving sustained release of antibiotics in the local sites of bone defects. In this work, the Ti6Al4V plates and CHACs were loaded with gentamicin in drug solutions with different doses of 150 μg and 300 μg, respectively. Fig. 4 shows the drug loading efficiencies of the Ti6Al4V plates and CHACs. The loading efficiency was the ratio of loaded amount of gentamicin to the initial amount of gentamicin after being washed by PBS. The CHACs exhibited the high drug loading efficiencies, which ranged from 80.83±4.23% to 81.18±4.52%, respectively. In contrast, the Ti6Al4V plates had less drug loading efficiency, which ranged from 1.40±0.17% to 2.20±0.15%. The remaining gentamicin amounts of Gent-Ti(150 μg) were almost the same as Gent-Ti(300 μg) after PBS washing. The drug loading efficiency of the CHACs was tremendous many times as great as that of the Ti6Al4V plates. The high gentamicin loading efficiencies achieved in the CHACs were attributed mainly to the following reasons. Firstly, the macropores and mesopores among or within carbonated hydroxyapatite plates not only decreased the diffusion limitation for drug delivery, but also provided space for loading drug. Our previous work reported that conventional hydroxyapatite particles without porous structures exhibited low drug loading efficiency of only 15.2~26.6%.[6b] Secondly, the CHACs possessed the great specific surface areas of 43.03 m^2/g, which increased the active

sits including OH^- and PO_4^{3-} groups. These functional groups could provide the carriers of great affinity towards gentamicin molecules. Finally, the low crystallinity of the CHACs played an important role in increasing the drug loading efficiency, too. As compared with the hydroxyapatite with a high crystallinity, the CHACs with a low crystallinity had more crystal defects that provided more active sites for adsorbing drug molecules.[22] In contrast, the Ti6Al4V plates exhibited a low drug loading efficiency because of no porous structure and low surface areas.

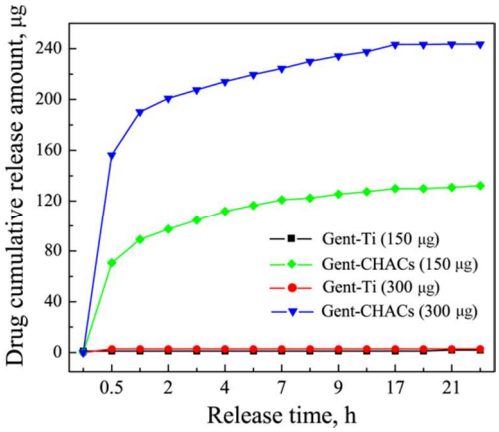

Fig. 5 The cumulative amounts of gentamicin released from Gent-Ti(150 μg), Gent-Ti (300 μg), Gent-CHACs(150 μg) and Gent-CHACs(300 μg)

The release amounts of gentamicin from the Gent-Ti and Gent-CHACs with time were analyzed by using the ophthaldialdehyde method. The *in vitro* gentamicin release profiles of the Gent-Ti and Gent-CHACs are shown in Fig. 5. There were obvious differences of the drug release trends among the Gent-Ti(150 μg), Gent-Ti(150 μg), Gent-CHACs(150 μg) and Gent-CHACs(300 μg). No gentamicin was released from both Gent-Ti(150 μg), Gent-Ti(150 μg) (Fig. 5), which might be attributed to the following two reasons. First, the Ti6Al4V plates had low drug-loading property, and few gentamicin was loaded in the substrates (Fig. 4). Secondly, gentamicin was adsorbed on the Ti6Al4V plates via physical adsorption, so most of gentamicin was washed away rapidly after soaking in PBS solutions. Interestingly, the Gent-CHACs(150 μg) and Gent-CHACs(300 μg) exhibited a relatively sustained release of gentamicin, which could prolong the drug effects up to 24 hours. The above two samples had a high drug release rates during the first 4 h, and then reached the release equilibrium upon increasing further release time (Fig. 5). From 5h to 24h, the concentrations of gentamicin released from the Gent-CHACs(150 μg) and Gent-CHACs (300 μg) still remained at about 18.0 μg/ml and 29.1 μg/ml, respectively. The concentrations were still greater than the effective antibacterial concentrations against *S. epidermidis* (ATCC35984). The effective drug release time was close to the needed time for prophylactic use of antibiotics in post operative treatment. The excellent drug release property achieved in the Gent-CHACs was attributed to the mesopores and macropores in the coatings. The hierarchically porous structures supported the drugs to enter into the entire coatings and release in a controlled manner. Moreover, the hydrogen bonding interactions between the coatings and drug molecules held back the rapid release of gentamicin from the Gent-CHACs.

3.3. Bactericidal property of Gent-CHACs

The Gent-CHACs exhibited good drug delivery property (Figs. 4 and 5), so they could be used as local antibiotic delivery systems to treat implant-associated infections. The bactericidal property of the Gent-CHACs was investigated by evaluating the bacteria adhesion and biofilm formation of *S. epidermis* (ATCC35984). Gent-Ti served as the control samples. The spread plate method was used to analyze antibacterial ability on the surface of samples. The number of viable bacteria was determined by the spread plate method, and was expressed as a number relative to that obtained from the pure Ti6Al4V plates. As shown in Fig. 6, there was no significant difference among the Ti6Al4V plates, Gent-Ti(150 μg), Gent-Ti(300 μg) and CHACs ($P > 0.05$). The Gent-HCACs (150 μg) and Gent-HCACs(300 μg) exhibited less colonies after culture for 24h than the other samples including the Ti6Al4V plates, Gent-Ti(150 μg), Gent-Ti(300 μg) and CHACs ($P < 0.05$). The relative numbers of viable bacteria (ATCC35984) on the CHACs, Gent-CHACs(150 μg) and Gent-CHACs(300 μg) were 1.0283, 0.0441 and 0.0078, respectively (Fig. 6b). According to the above results, the Ti6Al4V plates, Gent-Ti(150 μg), Gent-Ti(300 μg) and CHACs had no antibacterial property. The number of viable bacteria of ATCC35984 on the CHACs, Gent-CHACs(150 μg) and Gent-CHACs(300 μg) depended on the release of gentamicin from the drug carriers, and the order was as followed: CHACs > Gent-Gent-CHACs(150 μg) > Gent-CHACs(300 μg) (Fig. 6).

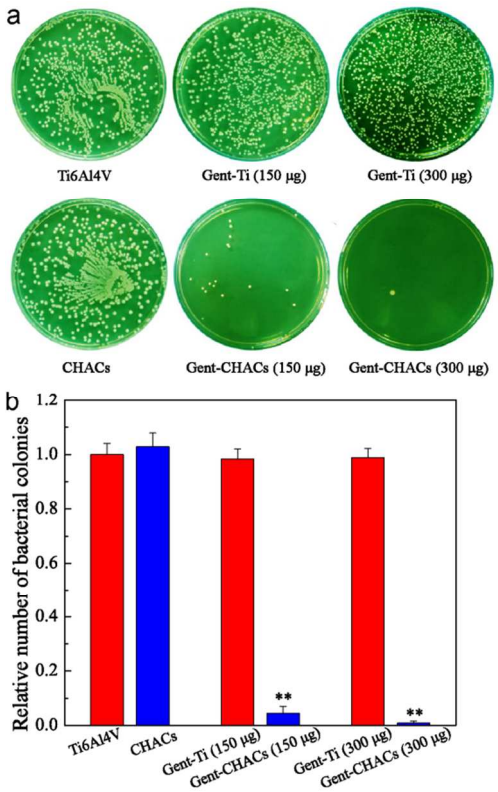

Fig. 6 (a) Representative images of viable bacteria grown on different samples after culturing for 24 h. (b) The relative number of viable bacteria of ATCC35984 on the different samples after culturing for 24 h was counted and normalized to the counts on Ti6Al4V plates. The data were represent as mean ± standard deviation; n=3. $^{**}P < 0.01$.

Fig. 7 shows the CLSM images of adherent bacteria stained by using the LIVE/DEAD Baclight bacteria viability kits. The viable cells with intact cell membranes stained fluorescent green, while nonviable cells with damaged membranes stained fluorescent red. A high intense level of green fluorescence on the surfaces of biomaterials indicated a high level of biofilm formation. As shown in Fig. 7, the intense level of fluorescence on the surfaces of the pure Ti6Al4V plates, Gent-Ti(150 μg), Gent-Ti(300 μg) and CHACs indicated a high level of biofilm formation. In addition, the level of biofilm formation on the different samples was followed as CHACs > Gent-CHACs(150 μg) > Gent-CHACs(300 μg), which was consistent with the number of viable bacteria (Fig. 6).

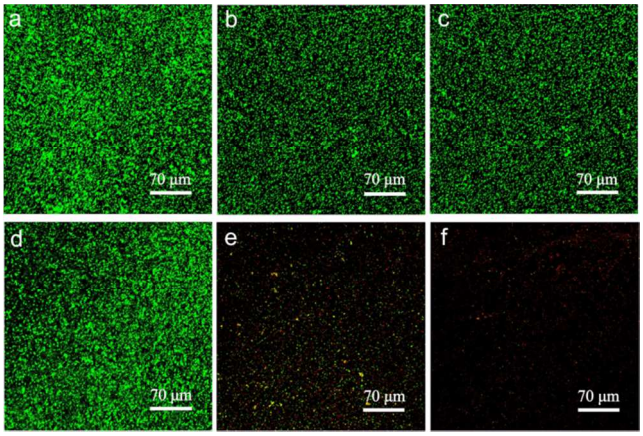

Fig. 7 CLSM image of bacteria on different samples after culturing for 24 h: (a) Ti6Al4V plates, (b) Gent-Ti(150 μg), (c) Gent-Ti (300 μg), (d) CHACs, (e) Gent-CHACs(150 μg) and (f) Gent-CHACs(300 μg). Bacteria were stained with green fluorescent SYTO 9 and red fluorescent propidium iodide, so live bacteria appeared green and dead bacteria appeared red.

Fig. 8 demonstrates the SEM images of bacteria on the surfaces of the Ti6Al4V plates and CHACs with or without loading gentamicin. The high bacterial adhesion on the Ti6Al4V plates, Gent-Ti(150 μg), Gent-Ti(300 μg) and CHACs was observed, whereas few bacterial adhesion presented on the Gent-CHACs(150 μg) and Gent-CHACs(300 μg). The scarce distribution of bacteria on the Gent-CHACs(150 μg) and Gent-CHACs(300 μg) confirmed further that the Gent-CHACs inhibited the bacterial growth against *S. epidermidis*. To learn if the antibiotic prevented the biofilm formation, the samples were stained by crystal violet. Absorption of crystal violet was used as an indicator of biofilm formation. The relative absorption of the crystal violet value was normalized to the pure Ti6Al4V plates at 2 h. When the culture time prolonged from 2 h to 8 h, significant increase in crystal violet staining was observed on the Gent-Ti(150 μg), Gent-Ti(300 μg) and CHACs. However, much less evidence of biofilm formation was detected on the Gent-CHACs(150 μg) and Gent-CHACs(300 μg). At all time points, crystal violet staining of the Gent-CHACs(150 μg) and Gent-CHACs(300 μg) was significant lower than the Gent-Ti(150 μg), Gent-Ti(300 μg) and CHACs, indicating that the Gent-CHACs prevented significantly the biofilm formation of *S. epidermidis*. (Fig. 9). The different bactericidal properties between the Gent-Ti and Gent-CHACs were attributed to their different drug loading-release properties. The CHACs exhibited a high drug loading efficiency of 80.83±4.23% to 81.18±4.52% because of their hierarchical porous structures (Figs. 2 and 4). Moreover, the sustained release of gentamicin from the Gent-CHACs reduced bacteria adhesion and biofilm formation (Fig. 5). In contrast, the gentamicin adsorbed on the Ti6Al4V plates released quickly before seeding bacteria on the samples, so many bacteria and biofilms were observed on the surfaces (Figs. 6-8).

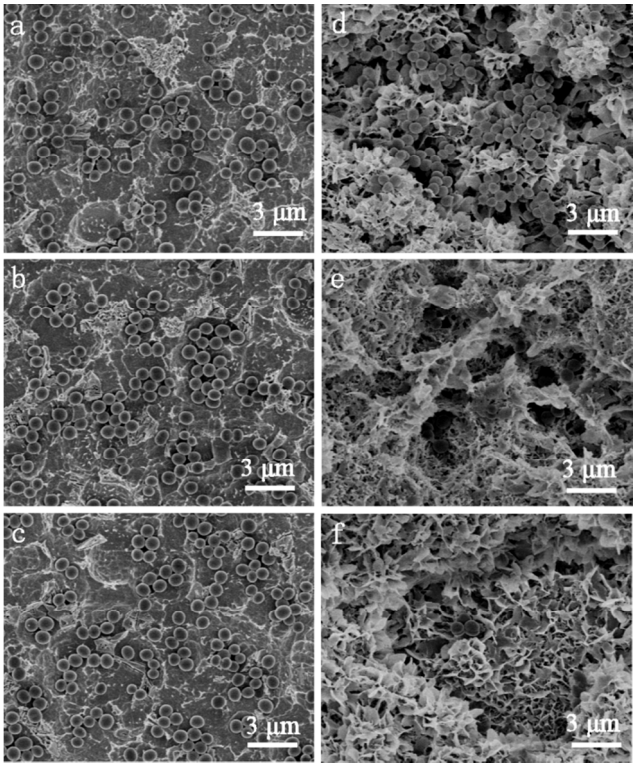

Fig.8 SEM image bacteria on different samples after culturing for 24 h: (a) Ti6Al4V plates, (b) Gent-Ti(150 μg), (c) Gent-Ti (300 μg), (d) CHACs,(e) Gent-CHACs(150 μg) and (f) Gent-CHACs(300 μg). The spherical particles in images are bacteria.

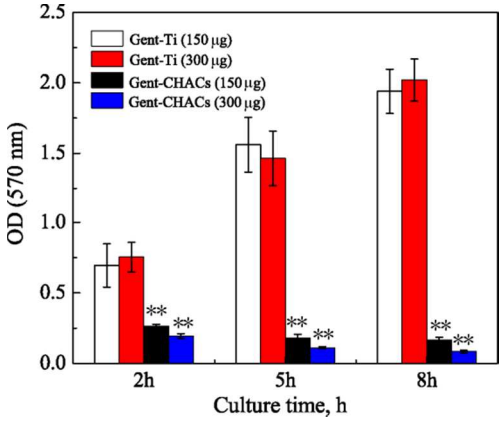

Fig. 9 Absorption of crystal violet was used as an indicator of biofilm formation by after culturing ATCC35984 for 2, 5 and 8 h. The data were represent as mean ± standard deviation; n=3. $^{**}P < 0.01$.

3.4. Biocompatibility of Gent-CHACs

The CHACs with hierarchically porous structures possessed excellent drug loading-release properties, so they had great potential for drug delivery systems to treat implant-associated infections. Previous works confirmed that conventional CHACs

could promote cell speading and proliferation,[23] but the effects of gentamicin released from Gent-CHACs on the biocompatibility was rarely investigated. In order to investigate *in vitro* biocompatibility of the Gent-CHACs, a series of biological experiments were carried out by using hBMSCs as cell models and using Ti6Al4V plates as control samples. Cytoskeleton analysis of the hBMSCs on the Ti6Al4V plates and Gent-CHACs(300 μg) was performed by using CLSM. The cytoskeleton is a highly dynamic network composed of actin polymers and a large variety of associated proteins. The function of the cytoskeleton is to mediate a variety of essential biological activities, including intra-cellular and extra-cellular movement and structural support. Orientation distribution of actin filaments within a cell is, therefore, an important determinant of cellular shape and functionality.[24] Fig. 10 shows the CLSCM images of the hBMSCs on the Ti6Al4V plates and Gent-CHACs(300 μg) after culturing for 24 h. Actin filaments were stained with TRITC phalloidin to image their orientation, and nuclei were stained with DAPI. The LSCM images revealed the long red bundles of stress fibers composed of actin filaments, displaying the good cell cytoskeleton morphology on both the Ti6Al4V plates and Gent-CHACs(300 μg) (Fig. 10). Notably, the cells on Gent-CHACs(300 μg) presented a clustering, confluency and multi-layering polygonal morphology at 24 h, while those on Ti6Al4V plates displayed a slim and fusiform-shaped morphology. Taken together, the hBMSCs on the Gent-CHACs(300 μg) had better cell adhesion, spreading and cell-cell contact than those on the Ti6Al4V plates.

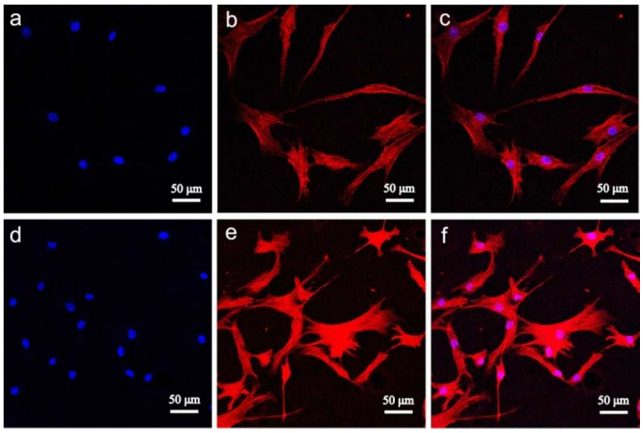

Fig. 10 CLSM images of hBMSCs cultured on different samples: (a-c) Ti6Al4V plates and (d-e) Gent-CHACs(300 μg). Representative images of cells stained with TRITC phalloidin for actin filaments (red) and nuclei stained with DAPI (blue).

CCK-8 assay is an effective method for testing mitochondrial impairment and correlates quite well with cell proliferation. Fig. 11 shows the CCK-8 assay results of hBMSCs growth on the Gent-CHACs(300 μg) by using the Ti6Al4V plates as control samples. The number of viable cells on both the Ti6Al4V plates and Gent-CHACs(300 μg) continued to increase with prolonging the culture time from 1 day to 7 days. For both samples, the cell number at 7 days was more than approximately four times that at 1 day (Fig. 11). The CLSM images and CCK-8 assay results suggested that both the Ti6Al4V plates and CHACs(300 μg) had excellent *in vitro* biocompatibility. Moreover, the number of viable cells on the Gent-CHACs (300 μg) was higher than that on the Ti6Al4V plates after culturing for 5 days and 7 days ($P < 0.01$), although there was no significant difference between two samples before culturing for 3 days. As compared with the Ti6Al4V plates, the CHACs(300 μg) exhibited better biocompatibility to promote the proliferation of hBMSCs (Fig. 11), which was attributed to the following reasons. Firstly, the main component of the CHACs was carbonated hydroxyapatite similar to bone minerals. Secondly, the CCHCs with hierarchically porous structures possessed the large contacting areas, which were preferable for the cell attachment, spreading and proliferation.[25] Moreover, the gentamicin released from Gent-CHACs was nontoxic to hBMSCs because of its small dosages.

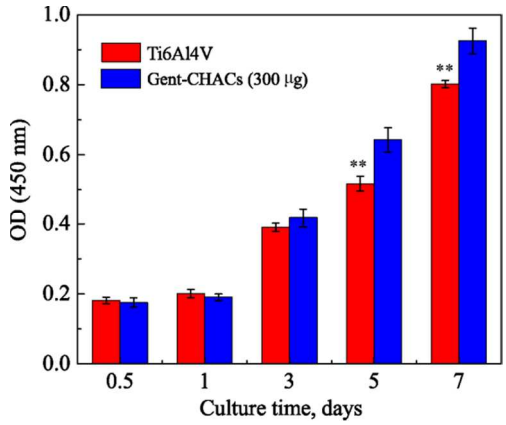

Fig. 11 CCK-8 assay results of hBMSCs growth on the Ti6Al4V plates and Gent-CHACs(300 μm) at different days. The data are represent as mean ± standard deviation; n=3. $^{**}P < 0.01$.

4. Conclusion

Gent-CHACs have been successfully fabricated according to the following steps: (i) formation of CHACs with hierarchically porous structures from CCCs by treatment with PBS, and (ii) loading gentamicin into the CHACs. The CHACs exhibit the hierarchical nanostructures constructed by plate-like particles as building blocks with mesopores and macropores. The hierarchically porous structures makes the CHACs possess higher drug loading-release properties than the Ti6Al4V plates. The controlled release of gentamicin from the Gent-CHACs can significantly diminish bacterial adhesion and prevent biofilm formation against *S. epidermidis* (ATCC35984). In addition, the *in vitro* cell tests demonstrate that the Gent-CHACs have better biocompatibility than the pure Ti6Al4V plates because of the hierarchically porous structures and similar chemical components to bone minerals. Moreover, the released gentamicin from the Gent-CHACs has no toxic effects on hBMSCs. The Gent-CHACs possess good biocompatibility, drug loading-release properties and bactericidal property, so they have great potentials as bone substitute materials to treat implant-associated infections.

Acknowledgements

This research was supported by Key Disciplines of Shanghai Municipal Education Commission (No. J50206), Natural Science Foundation of China (Nos. 51002095 and 51372152), Science and Technology Commission of Shanghai Municipality (No.

12JC1405600), Program of Shanghai Normal University (Nos. DZL124, DCL201303), Innovation Foundation of Shanghai Education Committee (No. 14ZZ124), and State Key Laboratory for Modification of Chemical Fibers and Polymer Materials, Dong Hua University.

Notes and references

[1] Sha Tang and Bo Tian contributed equally to this work.

[a] *The Education Ministry Key Lab of Resource Chemistry and Shanghai Key Laboratory of Rare Earth Functional Materials, Shanghai Normal University, Shanghai 200234, P. R. China. Fax: +86-21-64321951; Tel: +86-21-64321951; E-mail: ypguo@shnu.edu.cn (Y. P. Guo)*

[b] *Shanghai Key Laboratory of Orthopedic Implant, Department of Orthopedic Surgery, Shanghai Ninth People's Hospital, Shanghai Jiao Tong University School of Medicine, Shanghai 200011, China. E-mail: zhuzhenan2006@126.com (Z. A. Zhu)*

1 S. Kurtz, K. Ong, E. Lau, F. Mowat and M. Halpern, *J. Bone Joint Surg. Am.,* 2007, **89**, 780.

2 R. O. Darouiche, *N. Engl. J. Med.,* 2004, **350**, 1422.

3 (a) N. Chanchareonsook, H. Tideman, S. E. Feinberg, S. J. Hollister, L. Jongpaiboonkit, L. Kin and J. A. Jansen, *J. Biomed. Mater. Res. A* 2013, 101A, 2258; (b) X. Wei, C. Fu, K. Savino and M. Z. Yates, *Cryst. Growth Des.,* 2012, **12**, 3474; (c) W. Chen, T. Long, Y. J. Guo, Z. A. Zhu and Y. P. Guo, *J. Mater. Chem. B,* 2014, **2**, 1653; (d) W. Chen, T. Long, Y. J. Guo, Z. A. Zhu and Y. P. Guo, *RSC Adv.,* 2014, **4**, 185.

4 (a) M. Vallet-Regi, A. Rámila, R. P. del Real and J. Pérez-Pariente, *Chem. Mater.*, 2001, **13**, 308; (b) Y. F. Zhao, S.C. Loo and J. Ma, *J. Nanosci. Nanotechnol.*, 2009, **9**, 3720.

5 Z. Hou, P. Yang, H. Lian, L. Wang, C. Zhang, C. Li, R. Chai, Z. Cheng and J. Lin, *Chem. -Eur. J.*, 2009, **15**, 6973;

6 (a) Y. P. Guo, T. Long, S. Tang, Y. J. Guo and Z. A. Zhu, *J. Mater. Chem. B,* 2014, 2 2899; (b) T. Long, Y. P. Guo, S. Tang, Y. J. Guo and Z. A. Zhu, *RSC Adv.,* 2014, **4**, 11816; (c) C. Sui, Y. Lu, H. L. Gao, L. Dong, Y. Zhao, L. Ouali, D. Benczedi, H. Jerri and S. H. Yu, *Cryst. Growth Des.,* 2013, **13**, 3201; (d) T. Long, Y. P. Guo, Y. Z. Liu and Z. A. Zhu, RSC Adv., 2013, **3**, 24169; (e) C. Y. Yang, W. Guo, L. R. Cui, D. Xiang, K. Cai, H. M. Lin and F. Y. Qu, *Mater. Sci. Eng. C,* 2014, **36,** 237.

7 (a) C. Rey, *Biomaterials*, 1990, **11**, 3; (b) W. H. Yang, X. F. Xi, J. F. Li and K. Y. Cai, *Asian j. Chem.*, 2013, **25**, 3673.

8 (a) F. Jiang, D. P. Wang, S. Ye and X. Zhao, *J. Mater. Sci.-Mater. Med.,* 2014, **25**, 391; (b) F. Y. Zeng, J. Wang, Y. Wu, Y. M. Yu, W. Tang, M. L. Yin and C. S. Liu, *Colloid. Surface. A,* 2014, **441**, 737.

9 (a) W. Amer, K. Abdelouahdi, H. R. Ramananarivo, M. Zahouily, A. Fihri, K. Djessas, K. Zahouily, R. S. Varma and A. Solhy, *Crystengcomm*, 2014, **16**, 543; (b) W. Amer, K. Abdelouahdi, H. R. Ramananarivo, M. Zahouily, A. Fihri, Y. Coppel, R. S. Varma and A. Solhy, *Mater. Lett.,* 2013, 107, 189; (c) X. Y. Ye, S. Cai, G. H. Xu, Y. Dou and H. T. Hu, *Mater. Lett.,* 2012, **85**, 64.

10 (a) Y. Guo, Y. Zhou and D. Jia, *Acta Biomater.,* 2008, **4**, 334; (b) Y. Guo, Y. Zhou, D. Jia and Q. Meng, *Acta Biomater.,* 2008, **4**, 923.

11 (a) M. R.Virto, P. Frutos, S. Torrado and G. Frutos, *Biomaterials,* 2003, **24**, 79; (b) D.W. Lee, Y.P. Yun, K. Park and S. E. Kim, *Bone,* 2012, **50**, 974.

12 E. Com, E. Boitier, J. P. Marchandeau, A. Brandenburg, S. Schroeder, D. Hoffmann, A. Mally, J. C. Gautier, *Toxicol. Appl. Pharm.,* 2012, **258**, 124.

13 K. C. Popat, M. Eltgroth, T. J. Latempa, C. A. Grimes and T. A. Desai, *Biomaterials,* 2007, **28**, 4880.

14 P. Frutos Cabanillas, E. Diez Pena, J. M. Barrales-Rienda and G. Frutos, *Int. J. Pharmaceut.,* 2000, **209**, 15.

15 Y. Li, Y. Z. Liu, T. Long, X. B. Yu, T. T. Tang, K. R. Dai, B. Tian, Y. P. Guo, Z. A. Zhu, *J. Mater. Sci. Mater. Med.,* 2013, **24**, 1951.

16 G. A. O'Toole, L. A. Pratt, P. I. Watnick, D. K. Newman, V. B. Weaver and R. Kolter, *Method. Enzymol.,* 1999, **310**, 91.

17 H. Sun, C. Wu, K. Dai, J. Chang and T. Tang, *Biomaterials,* 2006, **27**, 5651.

18 (a) T. R. Rautray, R. Narayanan and K. H. Kim, *Prog. Mater. Sci.*, 2011, **56**, 1137; (b) J. S. Hayes and R. G. Richards, *Expert Rev. Med. Devices*, 2010, **7**, 843.

19 (a) J. Aizenberg, S. Weiner and L. Addadi, *Conn. Tiss. Res.*, 2003, **44**, 20; (b) J. Mahamid, B. Aichmayer, E. Shimoni, R. Ziblat, C. Li, S. Siegel, O. Paris, P. Fratzl, S. Weiner and L. Addadi, *PNAS*, 2010, **107**, 6316; (c) J. Seto, Y. Ma, S. A. Davis, F. Meldrum, A. Gourrier, Y. -Y. Kim, U. Schilde, M. Sztucki, M. Burghammer, S. Maltsev, C. Jäger and H. Cölfen, *PNAS,* 2012, **109**, 3699.

20 (a) M. Sivakumar, T. S. S. Kumar, K. L. Shantha and K. P. Rao, *Biomaterials,* 1996, 17, 1709; (b) W. L. Suchanek, K. Byrappa, P. Shuk, R. E. Riman, V. F. Janas and K. S. TenHuisen, *Biomaterials,* 2004, **25**, 4647; (c) C. B. Baddiel and E. E. Berry, *Spectrochim. Acta*, 1966, **22**,1407.

21 R. M. Wilson, S. E. P. Dowker, J. C. Elliott, *Biomaterials,* 2006, **27**, 4682.

22 A. Barroug, L. T. Kuhn, L. C. Gerstenfeld and M. J. Glimcher, *J. Orthop. Res.,* 2004, **22**, 703.

23 (a) Y. Dong, J. X. Yang, L. Q. Wang, X. Ma, Y. F. Huang, Z. Y. Qiu and F. Z. Cui, *J. Biomater. Appl.*, 2014, **2**, 990; (b) M. Li, Q. Liu, Z. J. Jia, X. C. Xu, Y. Cheng, Y. F. Zheng, T. F. Xi and S. C. Wei, *Carbon*, 2014, **67**, 185; (c) A. Hoppe, J. Will, R. Detsch, A. R. Boccaccini and P. Greil, *J. Biomed. Mater. Res. A,* 2014, **102**, 193.

24 J. Y. Rao, R. E. Hurst, W. D. Bales, P. L. Jones, R. A. Bass, L. T. Archer, P. B. Bell and G. P. Hemstreet, *Cancer Res.,* 1990, **50**, 2215.

25 (a)Y. Hong, H. Fan, B. Li, B. Guo, M. Liu and X. Zhang, *Mater. Sci. Eng. R*, 2010, **70**, 225; (b) X. Li, C.A. Blitterswijk, Q. Feng, F. Cui and F. Watari, *Biomaterials,* 2008, **29**, 3306.